Efficient Interpolation Method for Wireless Communications and Signal Processing Applications

Shu-Chen Lin, *Student Member, IEEE*, Kevin Chuang, *Senior Member, IEEE*, Chun-Wei Chang, *Member, IEEE*, and Jau-Horng Chen, *Senior Member, IEEE*

***Abstract*— Interpolation involves the process of estimating values at positions in between the adjacent samples, which has very fundamental and applied implications in signal processing and communication systems. In this work, a new method of cubic spline interpolation (CSI) is proposed and derived mathematically from the input samples respecting the time-domain boundary conditions, and the corresponding piecewise polynomials are optimized in the frequency domain to achieve good spectral properties. A comparative analysis of several prior arts, including arbitrary frequency response polynomial (AFRP) and basis spline (B-spline) is also presented, giving a clear overview of the advantages associated with the proposed technique in terms of implementation complexity, latency, and in-band and out-of-band spectral performance. The measurement results with three different radio frequency (RF) power amplifier (PA) prototypes using an input stimulus comprised of different instantaneous bandwidth (iBW) carrier aggregated 5G new radio (NR) waveform are demonstrated to highlight the improved performance in the context of digital predistortion (DPD) correction. Finally, the architecture of the proposed method is illustrated, which is suitable for real-time high-speed digital implementation.**

***Index Terms*— Cubic spline interpolation, filters, interpolation, microwave amplifier linearization techniques, power amplifiers (PAs).**

I. Introduction

THE concept of interpolation is widely adopted in many digital signal processing (DSP) applications. In image processing, for operations such as scaling [1], edge detection [2], motion compensation [3], and rendering [4], [5], the 2-D interpolation method is applied to obtain interpolated samples or a continuous function from original discrete samples, whereas in digital wireless communication system, the 1-D interpolation is essential for DSP, including sample rate conversion (SRC) [6], signal synchronization [7], and interpolated data access in lookup table (LUT)-based digital predistortion (DPD) [8]–[13]. In this work, we will demonstrate two examples of how the proposed interpolation method can be used to improve the performance of modern wireless transceiver systems: signal synchronization and DPD as highlighted in the system block diagram shown in Fig. 1.

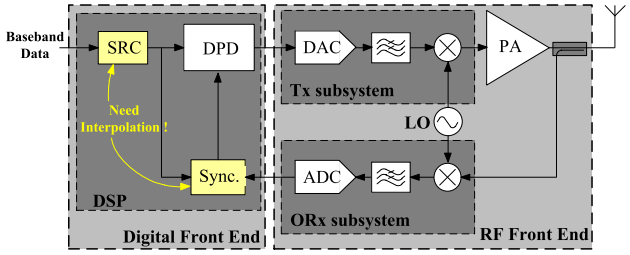

Fig. 1. Block diagram of a generic transmitter.

The purpose of interpolation is to estimate interpolated samples or a continuous function in between a set of existing samples. There are several intuitive implementations, such as nearest neighbor and linear interpolation, which require fewer computational resources at a cost of considerable approximation error. Accordingly, they are mostly applicable to high oversampling ratio (OSR) signals. In this work, OSR is defined as the ratio of data sampling rate to the instantaneous bandwidth (iBW). The limitation of OSR is undesirable in many use cases. As a result of that, various methods with higher accuracy have been proposed [14]–[17]. Among the proposed approaches, basis spline (B-spline) interpolation is one such method, which can be implemented efficiently in digital hardware systems for image processing applications [16]–[19]. In this approach, a noncausal infinite impulse response (IIR) is needed during the calculation. Since the images are mostly represented in finite samples, noncausal IIR operation can be achieved easily in such applications. In modern wireless communication systems, the signal is usually

Manuscript received October 21, 2020; revised December 31, 2020 and February 1, 2021; accepted February 2, 2021. Date of publication March 26, 2021; date of current version May 5, 2021. This work was supported in part by the Ministry of Science and Technology, Taiwan, under Grant MOST 109-2221-E-002-166-MY3 and Grant MOST 106-2221-E-002-222-MY3. *(Corresponding author: Shu-Chen Lin.)*

Shu-Chen Lin was with NanoSemi Inc., Waltham, MA 02451 USA. He is now with the Department of Engineering Science and Ocean Engineering, National Taiwan University, Taipei 10617, Taiwan (e-mail: f04525034@ntu.edu.tw).

Kevin Chuang is with NanoSemi, which is now part of MaxLinear, Waltham, MA 02451 USA (e-mail: kevinchuang@ieee.org).

Chun-Wei Chang was with the Department of Engineering Science and Ocean Engineering, National Taiwan University, Taipei 10617, Taiwan. He is now with NXP Semiconductors N. V., Chandler, AZ 85224 USA (e-mail: chunwei.chang@nxp.com).

Jau-Horng Chen is with the Department of Engineering Science and Ocean Engineering, National Taiwan University, Taipei 10617, Taiwan (e-mail: jauchen@ntu.edu.tw).

Color versions of one or more figures in this article are available at https://doi.org/10.1109/TMTT.2021.3061563.

Digital Object Identifier 10.1109/TMTT.2021.3061563

represented by infinite samples, which makes backward calculation in noncausal IIR filter not suitable. The most popular way for achieving signals time synchronization in a digital front-end system is by applying a low-pass filter (LPF) after the expanding operation [20]. Another attractive alternative is polynomial-based interpolating filters, and one of the methods is cubic spline interpolation (CSI). Compared to linear interpolation, the third-order piecewise polynomials are used in CSI to achieve a more accurate approximation [21]. A real-time implementation of CSI with a fixed moving window has been proposed in [22]. Another approach of polynomial-based interpolating filter is the arbitrary frequency response polynomial (AFRP) [23]–[26], where piecewise polynomials are used to represent finite impulse response (FIR) that can be optimized for desired frequency response through linear programming techniques [27]. Since the linearity requirement becomes more and more stringent in modern wireless communication systems, DPD is needed in both handset and base station devices [28]–[30]. Typically, time alignment with integer-sample accuracy is not sufficient for low OSR applications, so fractional time alignment is essential for DPD applications [31], [32]. Accordingly, an efficient interpolation technique can reduce the overall digital implementation cost. A new concept of CSI is first introduced through simulation in [33]. This article aims to explain the theory and its applications in detail with regard to the characteristics of a proposed polynomial-based method based on measurement results. It also demonstrates how the proposed polynomial-based method can be implemented efficiently by the Farrow structure [34].

II. Interpolation Methods and Theory

Consider a continuous time-varying signal $\hat{x}(t)$ that can be sampled into a discrete-time signal $x[n]$ as

$$x[n] = \hat{x}\left(\frac{n}{f_s}\right) \tag{1}$$

where n denotes the integer sample index from $-\infty$ to ∞, f_s is the sampling rate, and the corresponding sampling period is $T_s = 1/f_s$. The discrete sequence can be transformed to the frequency domain $X[\exp(j\omega)]$ by the Fourier transform operation $\mathfrak{F}(x[n])$, where ω is the angular frequency. Then, the Fourier transform of a time-shifted sequence $x[n - n_0]$ can be expressed as

$$\mathfrak{F}(x[n - n_0]) = e^{-j\omega n_0} X\left(e^{jw}\right). \tag{2}$$

As shown in (2), time delay is equivalent to phase shift in the frequency domain. Accordingly, the most straightforward way to align two digital sequences with unknown relative delay is to apply fast Fourier transform (FFT) and inverse fast Fourier transform (IFFT) to compensate for the phase offset in the frequency domain. However, it needs numerous computational resources and is rarely adopted for real-time applications. Therefore, it is more practical to time-align signals using interpolating filters [14].

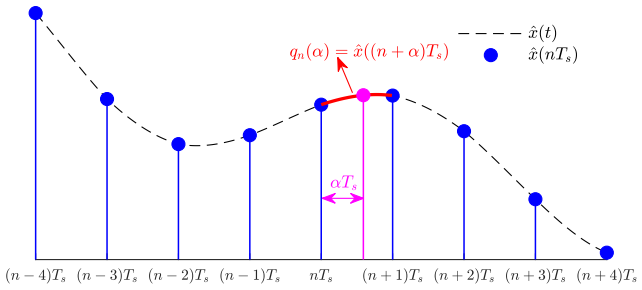

Fig. 2. Illustration of interpolating fractional sample.

A. Interpolation LPF

The upsampling of a signal $x[n]$ by a ratio L can be denoted as $x_L[n]$ as given by

$$x_L[n] = \begin{cases} x\left[\frac{n}{L}\right], & n = 0, \pm L \ldots \\ 0, & \text{otherwise.} \end{cases} \tag{3}$$

To remove unwanted aliasing components, it is essential to apply an LPF after the upsampling procedure. The digital LPF can be designed and implemented efficiently with an FIR filter, as shown in [14], [27], and [35].

B. Interpolating Polynomials

Another approach to interpolating filter is to use polynomial functions to reconstruct a continuous function $\hat{x}(t)$ from the discrete sequence $x[n]$. Because of the continuous waveform reconstruction, interpolating polynomials can be adopted for different interpolation precision without additional design overhead, unlike the FIR filter design.

To restore a continuous waveform from the discrete sequence $x[n]$, piecewise polynomials q_n are utilized for each sampling interval $nT_s \le t \le (n+1)T_s$, as shown in Fig. 2. The generalized form of q_n can be expressed as

$$q_n(\tau) = \sum_{m=-\infty}^{\infty} c[n+m]\psi^N(\tau - mT_s) \tag{4}$$

where $c[n]$ is the coefficient function, $\psi^N(t)$ indicates the Nth-order synthesis polynomial function, and τ is the time variable of each polynomial q_n within a sampling period defined as $\tau = (t - nT_s)/T_s$. According to Fig. 2 and (4), the interpolated samples can be obtained by inserting the desired fractional delay into each polynomial as

$$x[n + \alpha] = q_n(\alpha) \tag{5}$$

where the fractional delay α is bounded by $0 \le \alpha < 1$.

1) Cardinal B-Spline Interpolation: Cardinal B-spline interpolation uses B-spline as the synthesis function ψ^N in (4). The Nth-order B-spline function is defined in [36] as

$$B^N(t) = \sum_{n=0}^{N+1} \frac{(-1)^n}{L!} C_n^{L+1} (t - nT_s)^L u(t - nT_s) \tag{6}$$

where $u(t)$ is the step function and C_n^{L+1} is a combination defined as $(L+1)!/(L+1-n)!n!$. To satisfy the condition of

passing through all knot points, the coefficient function $c[n]$ can be obtained by digital convolution-inverse operation as shown in [37]

$$c[n] = \left(B^N(nT_s)\right)^{-1} * x[n] \tag{7}$$

where the Z transform $B^N(z)$ of B-spline function can be expressed as

$$B^N(z) = \sum_{n=0}^{N+1} B^N(nT_s) z^{-n}. \tag{8}$$

The cardinal B-spline interpolation can approximate an ideal sinc function with an order that approaches infinity [37]. However, the convolution-inverse operation in (7) cannot be implemented by a causal IIR, which results in higher computational complexity.

2) Cubic Spline Interpolation: Cubic spline interpolation solves the piecewise polynomials in time domain directly. Rewriting the q_n function in (4) as a classical third-order polynomial

$$q_{n,CSI}(\tau) = c_3[n]\tau^3 + c_2[n]\tau^2 + c_1[n]\tau + c_0[n] \tag{9}$$

where variables $c_3[n]$, $c_2[n]$, $c_1[n]$, and $c_0[n]$ in each monomial of (9) are the derived coefficients of each order in (4). As shown in [21], CSI defines the following conditions to solve these four variables:

$$q_{n,CSI}(0) = x[n]\ ,\ q_{n,CSI}(1) = x[n+1] \tag{10}$$
$$q'_{n,CSI}(1) = q'_{n+1,CSI}(0) \tag{11}$$
$$q''_{n,CSI}(1) = q''_{n+1,CSI}(0) \tag{12}$$

where (10) is the approximation curve that passes through all samples, and (11) and (12) are the continuous first derivative and second derivative, respectively. For a set of M samples, there exists $M-1$ polynomials, which is equivalent to $4M-4$ variables according to (9). Therefore, it needs two additional boundary conditions at the first and the last polynomials. Natural spline [21] is one such candidate, which defines zero edge second derivatives and can be expressed as

$$q''_{1,CSI}(0) = 0\ ,\ q''_{M-1,CSI}(1) = 0. \tag{13}$$

From the results of (9)–(13), each coefficient of the third-order polynomial can be solved as

$$c_3(n) = \frac{q''_{n+1,CSI}(0) - q''_{n,CSI}(0)}{6} \tag{14a}$$
$$c_2(n) = \frac{q''_{n,CSI}(0)}{2} \tag{14b}$$
$$c_1(n) = x[n+1] - x[n] - c_3(n) - c_2(n) \tag{14c}$$
$$c_0(n) = x[n] \tag{14d}$$

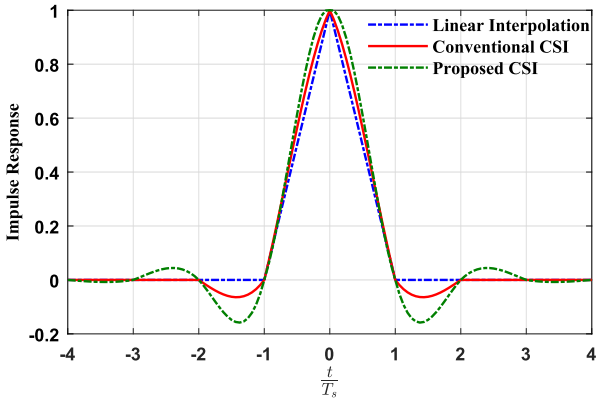

Fig. 3. Impulse response of linear interpolation, conventional four-point CSI, and proposed eight-point CSI.

where the second derivatives q''_n in (14a) and (14b) can be solved in matrix form directly as given by

$$\begin{bmatrix} 4 & 1 & 0 & \cdots & 0 \\ 1 & 4 & 1 & 0 & 0 \\ \vdots & \ddots & \ddots & \ddots & 0 \\ 0 & 0 & 1 & 4 & 1 \\ 0 & \cdots & 0 & 1 & 4 \end{bmatrix} \begin{bmatrix} q''_{2,CSI}(0) \\ q''_{3,CSI}(0) \\ \vdots \\ q''_{M-2,CSI}(0) \\ q''_{M-1,CSI}(0) \end{bmatrix} = 6 \begin{bmatrix} x[3] - 2x[2] + x[1] \\ x[4] - 2x[3] + x[2] \\ \vdots \\ x[M-1] - 2x[M-2] + x[M-3] \\ x[M] - 2x[M-1] + x[M-2] \end{bmatrix}. \tag{15}$$

To solve (15), all samples need to be collected first, which is not desirable for real-time implementation. Instead, a moving fixed-size window is employed in [22], which makes the computational resources of a real-time implementation reasonable. Although real-time CSI acquires fewer resources for implementation, it still suffers from the nonnegligible approximation error. The impulse responses and frequency responses of a linear interpolation and four-point ($M = 4$) CSI are shown in Figs. 3 and 4, respectively. The inadequate frequency filtering response shown in Fig. 4 would introduce unwanted aliasing error when the OSR is lower than a certain value [14]. If the passband rejection requirement is 40 dBc, the applicable operational bandwidth (BW) ratio of linear interpolation and CSI is $0.18f_s$ and $0.36f_s$, respectively, as shown in Fig. 4. Furthermore, de Carvalho and Hanson [22] shows that the OSR limitation of CSI cannot be improved by changing window size.

3) Arbitrary Frequency Response Polynomial: Vesma and Saramaki [23], Ridha *et al.* [24], and Vesma [25] proposed a new approach that uses piecewise polynomial functions to represent impulse response. By setting the coefficient function $c[n]$ to $x[n]$, (4) can be considered as an linear time-invariant (LTI) system with the corresponding impulse response ψ^N, consisted of piecewise Nth-order polynomials. In [25], the impulse response with finite sequence length, which continues $M \times T_s$ in the time domain, where

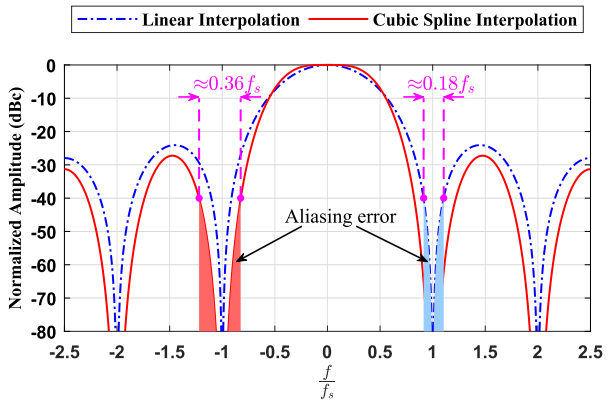

Fig. 4. Frequency response of linear interpolation and conventional four-point CSI.

TABLE I
LIST OF A_k, B_k, C_k AND D_k

	A_k	B_k	C_k	D_k
$k=-(\frac{M}{2}-1)$	$-\frac{a_{-k}}{6}$	$\frac{a_{-k}}{2}$	$-\frac{a_{-k}}{3}$	0
$k=-(\frac{M}{2}-2)\sim -1$	$\frac{a_{-k}-a_{-k+1}}{6}$	$\frac{a_{-k}}{2}$	$-\frac{a_{-k+1}+2a_{-k}}{6}$	0
$k=0$	$-\frac{a_1-a_0}{6}$	$\frac{a_0}{2}$	$-\frac{a_1+2a_0+6}{6}$	1
$k=1$	$-\frac{a_0-a_1}{6}$	$\frac{a_1}{2}$	$-\frac{a_0+2a_1-6}{6}$	0
$k=2\sim -(\frac{M}{2}-1)$	$\frac{a_{k-1}-a_k}{6}$	$\frac{a_k}{2}$	$-\frac{a_{k-1}+2a_k}{6}$	0
$k=\frac{M}{2}$	$\frac{a_{k-1}}{6}$	0	$-\frac{a_{k-1}}{6}$	0

M corresponds to M-point interpolation, is defined as

$$\psi^N(t)=\sum_{n=-\frac{M}{2}}^{\frac{M}{2}-1}\sum_{k=0}^{N}c_k(n)f_k(t-nT_s)$$
$$f_k(t)=\begin{cases}\left(\frac{2t}{T_s}-1\right)^k, & 0\le t<T_s\\ 0, & \text{otherwise.}\end{cases} \tag{16}$$

Because of the symmetry property, the desired frequency response can be obtained by optimizing $4L$ coefficients in (16). The biggest advantage of AFRP is the design flexibility of a given filter specification. However, it needs larger complexity compared to other methods.

III. Proposed Interpolation Method

The derivation of a novel CSI architecture is demonstrated in this section, aiming to improve the frequency response while maintaining the low-complexity and low-latency implementation. Inherited from the conventional CSI, the proposed method adopts the same continuous conditions from (14a)–(14d). However, instead of solving the matrix defined in (15), the proposed method uses a linear combination of neighboring samples with tunable coefficients a_k. For an M-sample interpolation with an even integer M, the second derivative of the

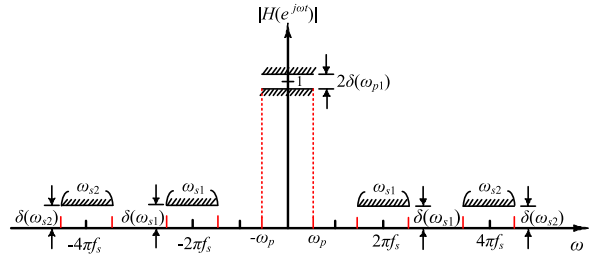

Fig. 5. Target frequency response with tolerance error $\delta(\omega)$.

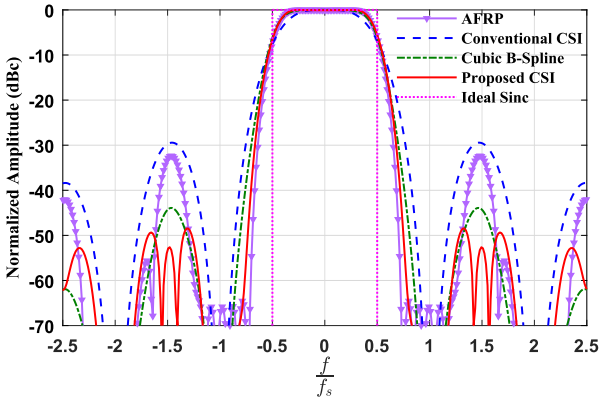

Fig. 6. Frequency response comparison of conventional CSI, cubic B-Spline interpolation, AFRP, proposed CSI, and ideal sinc function.

proposed method can be defined as

$$q_n''(0)=\sum_{k=-(\frac{M}{2}-1)}^{\frac{M}{2}-1}a_k x[n+k]. \tag{17}$$

Set the coefficients a_k real and even as

$$a_k=a_{-k} \tag{18}$$

where k is the coefficient index such that $1\le k\le M/2-1$. Substituting the second derivative (17) and (18) back to (14a)–(14d), the third-order polynomial can be expressed as

$$q_n(\tau)=\sum_{k=-(\frac{M}{2}-1)}^{\frac{M}{2}}x[n+k]F_k(\tau) \tag{19}$$

where $F_k(\tau)$ is a piecewise polynomial defined by

$$F_k(\tau)=A_k\tau^3+B_k\tau^2+C_k\tau+D_k \tag{20}$$

where A_k, B_k, C_k, and D_k are the coefficients for the third-order, second-order, linear, and constant terms, respectively. Table I summarizes how coefficients are obtained in order. From the results of (19) and (20) and Table I, the impulse response of the proposed method can be expressed as

$$h[n]=F_{\lfloor\frac{n}{L}\rfloor+1}\left(1-\frac{n\ (\text{mod}\ L)}{L}\right) \tag{21}$$

where L indicates the upsampling ratio and number of points $\{1,(L-1)/L,(L-2)/L,\ldots,1/L\}$ inserted into each polynomial function.

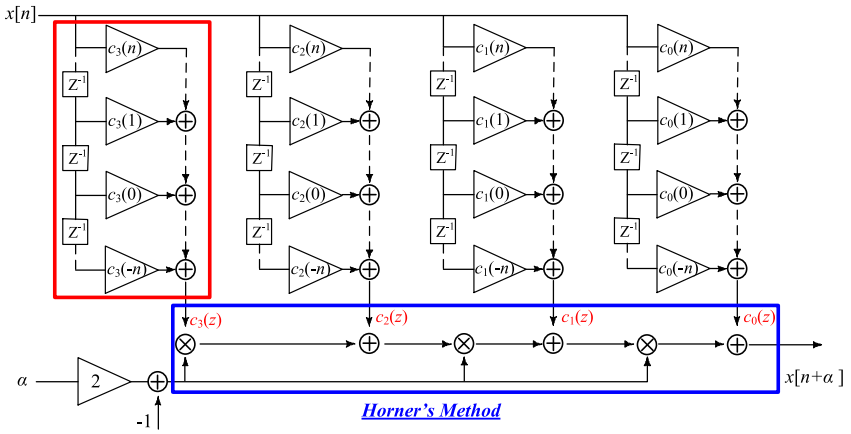

Fig. 7. Implementation block diagram of AFRP in [23]–[26].

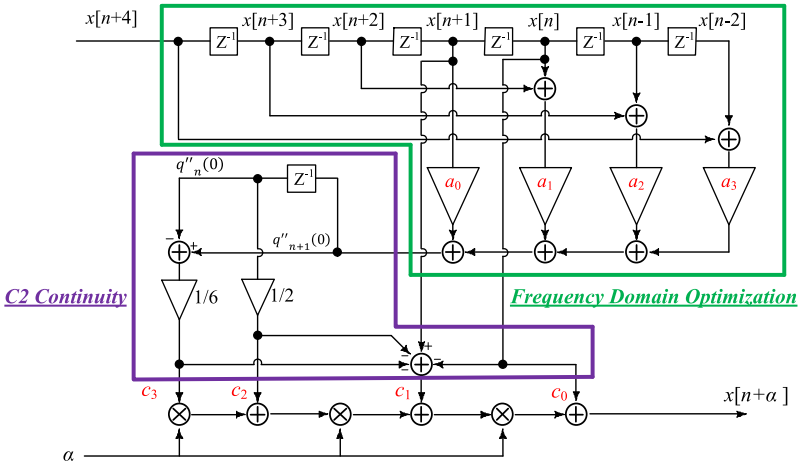

Fig. 8. Proposed CSI architecture.

After obtaining the impulse response of (21), the corresponding frequency response can be derived as

$$H\left(e^{j\omega}\right) = h[0] + 2\sum_{m=1}^{\frac{ML}{2}-1} h[m]\cos m\omega. \tag{22}$$

Because of the symmetry property in (18), only the positive response where $m \geq 0$ is concerned. From (17)–(22), it is shown that the corresponding frequency response $H[\exp(j\omega)]$ can be optimized by governing the coefficients between a_0 and $a_{M/2-1}$. Therefore, the spectral performance of the proposed CSI method can be improved to achieve the desired characteristics in the target frequency range. As shown in Fig. 5, for a band-limited signal with a cutoff frequency of ω_p, the frequency response $G[\exp(j\omega)]$ of the ideal interpolator has a unity gain in the passband $-\omega_p \leq \omega \leq \omega_p$ and infinite decay in the stopbands ω_{s1} and ω_{s2}. The goal of optimization is to approximate the frequency response $H[\exp(j\omega)]$ of the proposed CSI in (22) to the ideal response $G[\exp(j\omega)]$ respecting the target frequency range $\{\omega \in \mathbf{\Omega}\}$ until the difference is within the desired tolerance error δ. It can be expressed as

$$W(\omega)\left|\left(Ge^{j\omega}\right) - H\left(e^{j\omega}\right)\right| \leq \delta \tag{23}$$

where $W(\omega)$ is the weighting function and $\mathbf{\Omega}$ is the set of target frequency ranges. The optimized coefficients in (17) can be obtained by solving (23) with linear programming.

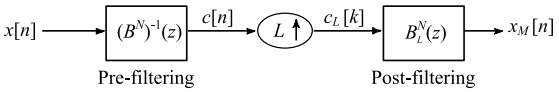

Fig. 9. Block diagram of L-order B-spline interpolation.

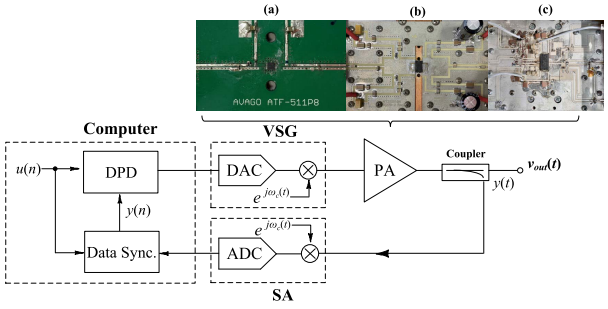

Fig. 10. Block diagram of the measurement setup using three different PA designs consisted of (a) class-AB pHEMT, (b) class-AB LDMOS, and (c) Doherty LDMOS power devices.

IV. Computational Complexity

In this work, we propose to use an eight-point ($M = 8$) CSI to provide sufficient flexibility for the frequency-domain optimization while maintaining low latency and low complexity. The corresponding coefficients $\{a_0, \ldots, a_3\}$ are optimized to

TABLE II
PERFORMANCE COMPARISON OF STATE-OF-THE-ART INTERPOLATION METHODS

	Computational Complexity				Approximation Error		
	Mutliplier (16x3)	Multiplier (16x16)	Adder	Latency	Passband (Edge at -0.5 dBc)	Stopband (Edge at -40 dBc)	Operational BW
Linear Interpolation	0	0	3	0	$0.13f_s$	$0.91f_s$	$0.18f_s$
Conventional CSI [1]	0	2	9	3	$0.23f_s$	$0.82f_s$	$0.36f_s$
AFRP	3	16	28	7	$0.36f_s$	$0.68f_s$	$0.64f_s$
Cubic B-Spline [2]	0	8	40	15	$0.32f_s$	$0.76f_s$	$0.48f_s$
Proposed CSI	3	5	13	7	$0.36f_s$	$0.71f_s$	$0.58f_s$

[1] Solving the second derivative by $M = 4$.
[2] Pre-filter is approximated by an 11-tap FIR [26]; post-filter is simplified by moving average filters as shown in [37].

be -4.9697, 3.1651, -0.7966, and 0.1185, respectively, and its impulse response is shown in Fig. 3. Moreover, the corresponding frequency response can be calculated according to (22). Fig. 6 shows the comparison between the proposed CSI, conventional CSI, AFRP in [23], cardinal cubic B-spline interpolation, and an ideal sinc interpolator that has a rectangular frequency response. It can be observed that the proposed CSI achieves a better in-band gain flatness and out-of-band suppression compared to conventional CSI.

In general, the DSP implementation of interpolation known as the Farrow structure [34] is widely adopted as an efficient architecture. For the implementation of AFRP, the modified Farrow structure is proposed in [23], which can be realized efficiently, as shown in Fig. 7. Horner's method highlighted in the bottom of Fig. 7 is used to solve the interpolated sample $q_n(\alpha)$ with a given fractional index α. Inherently, the proposed CSI can be implemented with a similar Farrow structure, as shown in Fig. 8. Compared to the same window size M, the proposed method only requires $M/2$ coefficients, which is just one fourth of the AFRP, suggesting that fewer multipliers and logic gates are needed. Moreover, the proposed method only needs one multiplier for every additional M.

The procedure of cardinal B-spline interpolation can be separated into prefiltering and postfiltering blocks as the overall block diagram shown in Fig. 9. The prefiltering block calculates the coefficient function $c[n]$ in (7) by convolution-inverse operation. The postfiltering block involves $c[n]$ and B-spline function expanding, which can be expressed as the following equations:

$$c_L[k] = \begin{cases} c[n], & k = Ln \\ 0, & \text{otherwise} \end{cases}, \quad B_L^N(t) = B^N\left(\frac{t}{L}\right) \tag{24}$$

where the convolution of two functions in (24) indicates the interpolated samples as defined in (7). It can either be completed by an FIR filter directly as shown in [18] or simplified to an L-times repeatedly moving average filter before a low-cost B-spline filter as shown in [37]. On the other hand, the transfer function of the prefiltering block is derived in [37], which has been shown that the poles are reciprocal pairs $\{\alpha, \alpha - 1\}$ for every order N. In other words, the prefiltering block cannot be implemented by a casual stable IIR, where the necessary condition is every pole being inside the unit circle. It needs an additional noncausal IIR that requires backward calculation as shown in [38]. Otherwise, it can be approximated by an FIR filter, which needs a relatively larger amount of multiplications [26]. As a result, the proposed

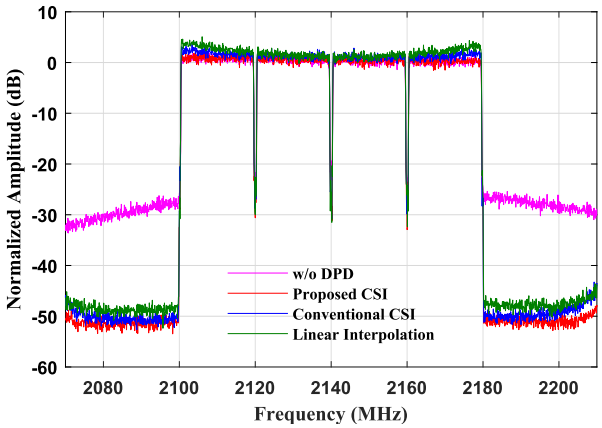

Fig. 11. Measured output spectrum comparison of class-AB LDMOS PA with different interpolation methods.

CSI provides the lowest computational complexity over other techniques with operational BW greater than $0.4f_s$, as summarized in Table II. The implementation resources are estimated with $8\times$ upsampling ratio ($L = 8$) and 16-bit data precision conditions. All computations shown in Table II are assumed to be done sequentially, which means that the number of blocks is equal to the number of operations. As shown in [37, Fig. 2], postfilter $B_8^3(z)$ can be simplified to

$$B_8^3(z) = \left(\frac{1}{8^3} B_8^0 * B_8^0 * B_8^0 * B_8^0(z)\right) * B_1^3(z). \tag{25}$$

Each $B_8^0(z)$ can be considered as a moving average filter, and $B_1^3(z)$ can be implemented by a three-tap FIR filter. The comparison of approximation error for each interpolation method is also presented in Table II. It is worthwhile to note that an ideal interpolator exhibits 0 dB attenuation in-band and ∞ dB suppression at $0.5f_s$ edge. Unlike other prior methods as shown in Table II, the proposed CSI achieves sufficient accuracy with operational BW up to $0.58f_s$ while meeting a stopband rejection of 40 dBc.

V. MEASUREMENT RESULTS

To evaluate the performance of the proposed interpolation method, a wireless transmitter line-up at 2140-MHz radio frequency (RF) frequency is prepared. The system block diagram is shown in Fig. 10 where the interpolation is utilized in the signal synchronization block. The baseband signal is loaded to a vector signal generator (VSG) in the TX path and downconverted to the baseband by a spectrum analyzer (SA) in the RX path with a sampling frequency

TABLE III
PERFORMANCE COMPARISON UNDER DIFFERENT CONDITIONS

PA Technology	iBW	Techniques	ACLR (dBc)	EVM (%)	Maximal in-band PSD error (dBc)
Class-AB pHEMT (@ P_{out} = 16.5 dBm)	60 MHz	With no correction	-36.6	2.0	-17
		Linear Interpolation + DPD	-50.3	1.4	-27
		Conventional CSI + DPD	-51.4	1.4	-31
		Proposed CSI + DPD	-51.9	1.3	-44
Class-AB LDMOS (@ P_{out} = 30.9 dBm)	60 MHz	With no correction	-27.8	5.2	-26
		Linear Interpolation + DPD	-51.2	1.4	-24
		Conventional CSI + DPD	-52.4	1.2	-35
		Proposed CSI + DPD	-51.9	1.2	-46
Class-AB LDMOS (@ P_{out} = 30.9 dBm)	80 MHz	With no correction	-28.0	5.7	-27
		Linear Interpolation + DPD	-50.9	1.3	-22
		Conventional CSI + DPD	-51.7	1.2	-29
		Proposed CSI + DPD	-51.8	1.2	-41
Doherty LDMOS (@ P_{out} = 38.0 dBm)	80 MHz	With no correction	-24.1	7.8	-19
		Linear Interpolation + DPD	-48.3	1.3	-22
		Conventional CSI + DPD	-53.1	1.2	-25
		Proposed CSI + DPD	-53.1	1.2	-46

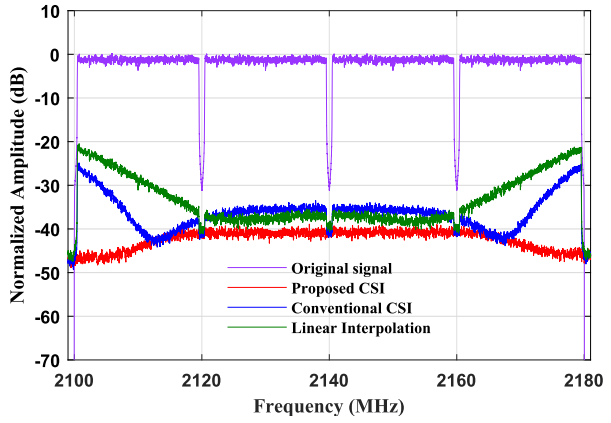

Fig. 12. Measured in-band PSD error comparison of Doherty LDMOS PA with different interpolation methods.

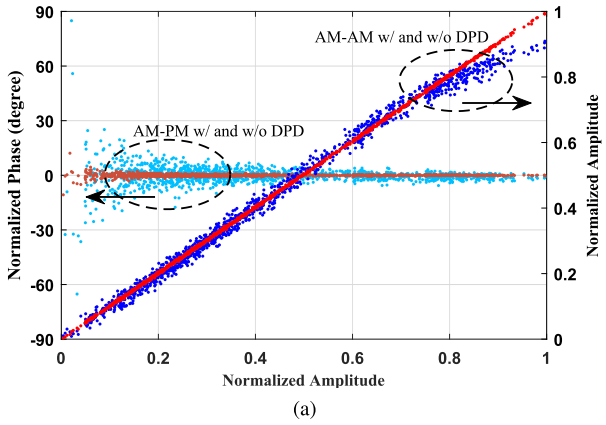

Fig. 13. AM-AM and AM-PM characteristics of (a) class-AB pHEMT and (b) class-AB LDMOS PA with DPD (red line) and without DPD (blue line) using 60-MHz carrier-aggregated 5G NR signal.

of 150 MHz. The measurement is performed on three different power amplifiers (PAs). Two of them are class-AB PAs that are designed with an NXP AFT20S15N LDMOS transistor and an Avago ATF-511P8 enhancement-mode pHEMT, respectively. The third prototype is a commercial Doherty PA designed with the NXP A2I20H060NR1 LDMOS transistor. Two different carrier configurations featuring signal aggregation of multiple 5G new radio (NR) 1024-QAM 20-MHz component carriers are used in the measurement. The crest factor reduction (CFR) is applied on the input signal to achieve a 9-dB peak-to-average power ratio (PAPR). In order to assess the impact of interpolation accuracy on the performance of linearized wireless transmitter chain, an iterative-learning-control (ILC) DPD correction technique [39] is used in conjunction with different interpolation approaches. Note that all the DSP functions and techniques discussed in this article are modeled and evaluated in MATLAB. The measurement results are shown in Figs. 11 and 12 and Table III. The AM-AM and AM-PM characteristics of 60- and 80-MHz measurements with and without DPD are shown in Figs. 13 and 14, respectively. Note that Doherty PA can achieve 37.5% drain efficiency at 9-dB back-off. From Table III, it can be seen that linear interpolation achieves the worst out-of-band and in-band performance, which can be demonstrated by adjacent channel leakage ratio (ACLR) and error vector magnitude (EVM), respectively. To further analyze in-band performance, the measured power spectral density (PSD) error is shown in Fig. 12. In this example, the measurement result demonstrates a low OSR (i.e., 80/150 $= 0.53 f_s$). It can also be seen from Table III that the proposed method achieves in-band PSD error as low as -46 dB at the edge of passband, whereas the conventional CSI and linear interpolation can only achieve -25 and -22 dB, respectively. Consequently, the subcarriers at the edge of passband could

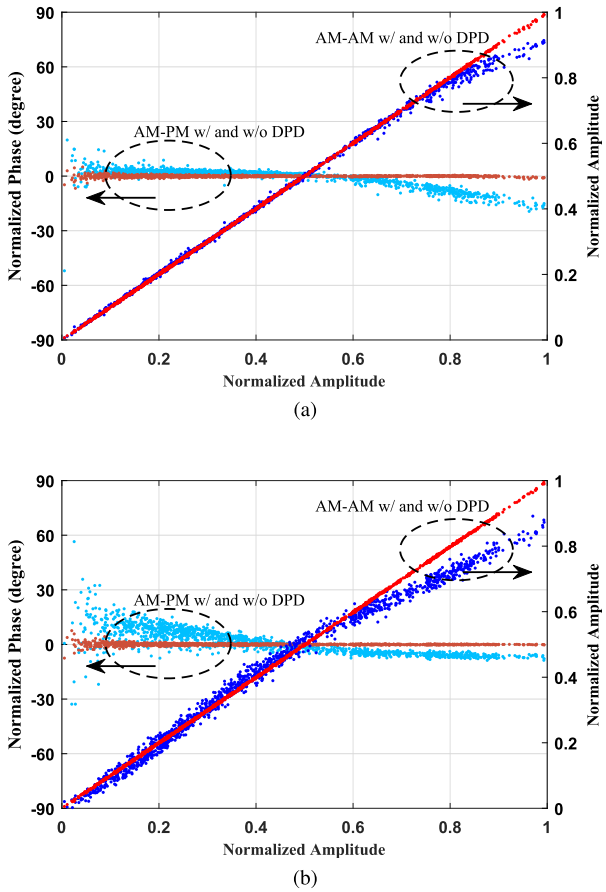

Fig. 14. AM-AM and AM-PM characteristics of (a) class-AB LDMOS and (b) Doherty LDMOS PA with DPD (red line) and without DPD (blue line) using 80-MHz carrier-aggregated 5G NR signal.

be affected with the conventional CSI and linear interpolation methods. Furthermore, according to the aforementioned results shown in Figs. 4 and 6, the frequency response near Nyquist rate suffers greatly from attenuation and aliasing. Therefore, any operation near the Nyquist frequency is inaccurate and thus can be ignored. Even though the PSD error near the Nyquist rate is progressively worse, the level of aliasing error is still inadequate to damage the spectral improvement, as shown in Fig. 11.

VI. Conclusion

In this work, a new method of interpolation is derived analytically and proposed for higher performance and ease of real-time implementation. Compared to the conventional CSI, the proposed method improves the frequency-domain properties significantly while maintaining low complexity. A design example of eight-point CSI is demonstrated and compared to conventional polynomial-based interpolation techniques. The results indicate that the proposed CSI has adequate approximation accuracy for signal synchronization application in modern wireless communication systems while having the lowest computational complexity. The measurement of a low OSR application shows that the proposed synchronization method can achieve the best in-band flatness and EVM performance compared to linear interpolation and conventional CSI.

References

[1] J. Shi and S. E. Reichenbach, "Image interpolation by two-dimensional parametric cubic convolution," *IEEE Trans. Image Process.*, vol. 15, no. 7, pp. 1857–1870, Jul. 2006.
[2] L. Romani, M. Rossini, and D. Schenone, "Edge detection methods based on RBF interpolation," *J. Comput. Appl. Math.*, vol. 349, pp. 532–547, Mar. 2019.
[3] H. Lakshman, H. Schwarz, and T. Wiegand, "Generalized interpolation-based fractional sample motion compensation," *IEEE Trans. Circuits Syst. Video Technol.*, vol. 23, no. 3, pp. 455–466, Mar. 2013.
[4] A. Guetat, A. Ancel, S. Marchesin, and J.-M. Dischler, "Pre-integrated volume rendering with non-linear gradient interpolation," *IEEE Trans. Vis. Comput. Graphics*, vol. 16, no. 6, pp. 1487–1494, Nov. 2010.
[5] S. Lee, G. Jounghyun Kim, and S. Choi, "Real-time depth-of-field rendering using anisotropically filtered mipmap interpolation," *IEEE Trans. Vis. Comput. Graphics*, vol. 15, no. 3, pp. 453–464, May 2009.
[6] X. Huang, Y. J. Guo, and J. A. Zhang, "Sample rate conversion using B-Spline interpolation for OFDM based software defined radios," *IEEE Trans. Commun.*, vol. 60, no. 8, pp. 2113–2122, Aug. 2012.
[7] T.-B. Deng, "Discretization-free design of variable fractional-delay FIR digital filters," *IEEE Trans. Circuits Syst. I, Reg. Papers*, vol. 48, no. 6, pp. 637–644, Jun. 2001.
[8] S. Boumaiza, J. Li, M. Jaidane-Saidane, and F. M. Ghannouchi, "Adaptive digital/RF predistortion using a nonuniform LUT indexing function with built-in dependence on the amplifier nonlinearity," *IEEE Trans. Microw. Theory Techn.*, vol. 52, no. 12, pp. 2670–2677, Dec. 2004.
[9] K.-F. Liang, J.-H. Chen, and Y.-J.-E. Chen, "A quadratic-interpolated LUT-based digital predistortion technique for cellular power amplifiers," *IEEE Trans. Circuits Syst. II, Exp. Briefs*, vol. 61, no. 3, pp. 133–137, Mar. 2014.
[10] A. Molina, K. Rajamani, and K. Azadet, "Concurrent dual-band digital predistortion using 2-D lookup tables with bilinear interpolation and extrapolation: Direct least squares coefficient adaptation," *IEEE Trans. Microw. Theory Techn.*, vol. 65, no. 4, pp. 1381–1393, Apr. 2017.
[11] A. Molina, K. Rajamani, and K. Azadet, "Digital predistortion using lookup tables with linear interpolation and extrapolation: Direct least squares coefficient adaptation," *IEEE Trans. Microw. Theory Techn.*, vol. 65, no. 3, pp. 980–987, Mar. 2017.
[12] Q. A. Pham, D. Lopez-Bueno, T. Wang, G. Montoro, and P. L. Gilabert, "Partial least squares identification of multi look-up table digital predistorters for concurrent dual-band envelope tracking power amplifiers," *IEEE Trans. Microw. Theory Techn.*, vol. 66, no. 12, pp. 5143–5150, Dec. 2018.
[13] J. Ren, "Digital predistorter for short-wave power amplifier with improving index accuracy of lookup table based on FPGA," *IEEE Access*, vol. 7, pp. 182881–182885, Dec. 2019.
[14] R. W. Schafer and L. R. Rabiner, "A digital signal processing approach to interpolation," *Proc. IEEE*, vol. 61, no. 6, pp. 692–702, Jun. 1973.
[15] H. Hou and H. Andrews, "Cubic splines for image interpolation and digital filtering," *IEEE Trans. Acoust., Speech, Signal Process.*, vol. 26, no. 6, pp. 508–517, Dec. 1978.
[16] M. Unser, A. Aldroubi, and M. Eden, "B-spline signal processing. I. Theory," *IEEE Trans. Signal Process.*, vol. 41, no. 2, pp. 821–833, Feb. 1993.
[17] M. Unser, A. Aldroubi, and M. Eden, "B-spline signal processing. II. Efficiency design and applications," *IEEE Trans. Signal Process.*, vol. 41, no. 2, pp. 834–848, Feb. 1993.
[18] L. Kai-Yu, W. Wen-Dong, Z. Kai-Wen, L. Wen-Bo, and X. Gui-Li, "The application of B-spline based interpolation in real-time image enlarging processing," in *Proc. 2nd Int. Conf. Syst. Informat. (ICSAI)*, Shanghai, China, Nov. 2014, pp. 823–827.
[19] S. Abbas, M. Irshad, and M. Z. Hussain, "Adaptive image interpolation technique based on cubic trigonometric B-spline representation," *IET Image Process.*, vol. 12, no. 5, pp. 769–777, May 2018.
[20] H. Keung Kwan and A. Jiang, "FIR, allpass, and IIR variable fractional delay digital filter design," *IEEE Trans. Circuits Syst. I, Reg. Papers*, vol. 56, no. 9, pp. 2064–2074, Sep. 2009.
[21] S. A. Dyer and J. S. Dyer, "Cubic-spline interpolation: Part 1," *IEEE Instrum. Meas. Mag.*, vol. 4, no. 1, pp. 44–46, Mar. 2001.
[22] J. M. de Carvalho and J. V. Hanson, "Real-time interpolation with cubic splines and polyphase networks," *Can. Electr. Eng. J.*, vol. 11, no. 2, pp. 64–72, Apr. 1986.
[23] J. Vesma and T. Saramaki, "Interpolation filters with arbitrary frequency response for all-digital receivers," in *Proc. IEEE Int. Symp. Circuits Syst.*, Atlanta, GA, USA, May 1996, pp. 568–571.

[24] H. Ridha, J. Vesma, T. Saramaki, and M. Renfors, "Derivative approximations for sampled signals based on polynomial interpolation," in *Proc. 13th Int. Conf. Digit. Signal Process.*, Santorini, Greece, 1997, pp. 939–942.
[25] J. Vesma, "A frequency-domain approach to polynomial-based interpolation and the farrow structure," *IEEE Trans. Circuits Syst. II, Analog Digit. Signal Process.*, vol. 47, no. 3, pp. 206–209, Mar. 2000.
[26] J. Vesma and T. Saramaki, "Polynomial-based interpolation Filters—Part I: Filter synthesis," *Circuits, Syst. Signal Process.*, vol. 26, no. 2, pp. 115–146, Apr. 2007.
[27] T. Baran, D. Wei, and A. V. Oppenheim, "Linear programming algorithms for sparse filter design," *IEEE Trans. Signal Process.*, vol. 58, no. 3, pp. 1605–1617, Mar. 2010.
[28] Y. Ma, Y. Yamao, Y. Akaiwa, and C. Yu, "FPGA implementation of adaptive digital predistorter with fast convergence rate and low complexity for multi-channel transmitters," *IEEE Trans. Microw. Theory Techn.*, vol. 61, no. 11, pp. 3961–3973, Nov. 2013.
[29] Q. A. Pham, G. Montoro, D. Lopez-Bueno, and P. L. Gilabert, "Dynamic selection and estimation of the digital predistorter parameters for power amplifier linearization," *IEEE Trans. Microw. Theory Techn.*, vol. 67, no. 10, pp. 3996–4004, Oct. 2019.
[30] C. D. Presti, D. F. Kimball, and P. M. Asbeck, "Closed-loop digital predistortion system with fast real-time adaptation applied to a handset WCDMA PA module," *IEEE Trans. Microw. Theory Techn.*, vol. 60, no. 3, pp. 604–618, Mar. 2012.
[31] J. Kral, T. Gotthans, and M. Harvanek, "Analytical method of fractional sample period synchronisation for digital predistortion systems," in *Proc. 27th Int. Conf. Radioelektronika (RADIOELEKTRONIKA)*, Apr. 2017, pp. 1–5.
[32] S. Traverso and J.-Y. Bernier, "Low complexity time synchronization based on digital predistortion coefficients," *IEEE Microw. Wireless Compon. Lett.*, vol. 29, no. 3, pp. 240–242, Mar. 2019.
[33] S.-C. Lin, K. Chuang, and J.-H. Chen, "Efficient implementation of cubic spline interpolator," in *Proc. IEEE Radio Wireless Symp. (RWS)*, San Antonio, TX, USA, Jan. 2020, pp. 287–290.
[34] C. W. Farrow, "A continuously variable digital delay element," in *Proc. IEEE . Int. Symp. Circuits Syst.*, vol. 3, Espoo, Finland, Jun. 1988, pp. 2641–2645.
[35] T.-B. Deng, S. Chivapreecha, and K. Dejhan, "Bi-minimax design of even-order variable fractional-delay FIR digital filters," *IEEE Trans. Circuits Syst. I, Reg. Papers*, vol. 59, no. 8, pp. 1766–1774, Aug. 2012.
[36] L. L. Schumaker, *Spline Functions: Basic Theory*. New York, NY, USA: Wiley, 1981.
[37] M. Unser, A. Aldroubi, and M. Eden, "Fast B-spline transforms for continuous image representation and interpolation," *IEEE Trans. Pattern Anal. Mach. Intell.*, vol. 13, no. 3, pp. 277–285, Mar. 1991.
[38] J. T. Olkkonen and H. Olkkonen, "Fractional delay filter based on the B-spline transform," *IEEE Signal Process. Lett.*, vol. 14, no. 2, pp. 97–100, Feb. 2007.
[39] J. Chani-Cahuana, P. N. Landin, C. Fager, and T. Eriksson, "Iterative learning control for RF power amplifier linearization," *IEEE Trans. Microw. Theory Techn.*, vol. 64, no. 9, pp. 2778–2789, Sep. 2016.

Shu-Chen Lin (Student Member, IEEE) received the B.S. degree in engineering science and ocean engineering from National Taiwan University, Taipei, Taiwan, in 2015, where he is currently pursuing the Ph.D. degree.

From 2015 to 2018, he was a Research Assistant with the Department of Engineering Science and Ocean Engineering, where he was involved in RF power amplifiers linearization for 4G/5G wireless infrastructure. From 2019 to 2020, he was an Intern Engineer with NanoSemi, Inc. Waltham, MA, USA. His current research interests include the use of signal processing strategies for linearity improvement of RF power amplifiers and high-efficiency transmitters in wireless communication systems.

Kevin Chuang (Senior Member, IEEE) was born in Taipei, Taiwan, in 1985. He received the B.S. degree (Hons.) in electrical engineering from the University of California at Santa Barbara (UCSB), Santa Barbara, CA, USA, in 2007, and the M.S. and Ph.D. degrees in electrical and computer engineering from the Georgia Institute of Technology, Atlanta, GA, USA, in 2009 and 2011, respectively.

From 2011 to 2014, he was a Member of Technical Staff with the MIT Lincoln Laboratory, Lexington, MA, USA, where he developed RF and mixed-signal ICs for high-linearity receivers and transmitters in multiple system-on-a-chip (SoC) design cycles. In 2014, he co-founded NanoSemi, Inc. Waltham, MA, USA, which was subsequently acquired by MaxLinear, Waltham, MA, USA, in 2020, where he was a Domain Leader in RF Systems and pioneered the development of wideband linearization systems. From May 2020 to October 2020, he was a Lead RF Systems Engineer with Wafer, LLC, Beverly, MA, USA, developing distributed electronically steerable array systems for satellite communications. Since 2020, he has been a Senior Principal Systems Engineer with MaxLinear, working on the radio development for wireless infrastructure. His technical contributions are at the intersection of wireless communications, RF electronics, and signal processing algorithms. His research interests are focused on the characterization and linearization of nonlinear communication systems, including RF power amplifiers.

Dr. Chuang is a member of Tau Beta Pi, Eta Kappa Nu, and the National Society of Collegiate Scholars. He is also the General Chairman of the 2022 IEEE Radio and Wireless Week. He was a recipient of the 2007 Joseph J. Sayovitz Scholarship for outstanding achievement in electrical engineering at UCSB. He serves on the Executive Committee of the IEEE Radio and Wireless Week and the IEEE MTT-S Boston Section.

Chun-Wei Chang (Member, IEEE) received the M.S. and Ph.D. degrees in engineering science and ocean engineering from National Taiwan University, Taipei, Taiwan, in 2011 and 2018, respectively.

From 2011 to 2014, he was a Design Engineer with Richwave Technology, Taipei, where he was involved in designing RF components and CMOS FM receivers. From 2015 to 2017, he was an Intern Design Engineer with NXP Semiconductors N. V., Chandler, AZ, USA, where he was involved in designing high-power RF power amplifiers for 4G/5G wireless infrastructure. In 2018, he joined NXP Semiconductors N. V., where he is currently an RF/Wireless Development Engineer. He holds two issued U.S. and foreign patents. His current research interests include analog/RF IC design, advanced receiver/transmitter architectures, and power amplifier (PA) linearization techniques for cellular networks.

Jau-Horng Chen (Senior Member, IEEE) received the B.S. degree in electrical engineering from National Taiwan University, Taipei, Taiwan, in 2001, and the M.S. and Ph.D. degrees in electrical and computer engineering from the Georgia Institute of Technology, Atlanta, GA, USA, in 2002 and 2006, respectively.

From 2006 to 2008, he was a Design Engineer with Freescale Semiconductor, Tempe, AZ, USA, where he was involved in designing dc–dc converters and digital predistortion linearizers for cell phone power amplifiers (PAs). In 2008, he returned to National Taiwan University, where he is currently a Full Professor and the Associate Chair of the Department of Engineering Science and Ocean Engineering. He holds five U.S. patents. His current research interests include analog/RF IC design, high-efficiency PAs, and field-programmable gate array (FPGA) prototyping.